Theoretical study of phosphorescence in dye doped light emitting diodes

ARTICLE *in* THE JOURNAL OF CHEMICAL PHYSICS · JANUARY 2007

Impact Factor: 2.95 · DOI: 10.1063/1.2388263 · Source: PubMed

Available online at www.sciencedirect.com
ScienceDirect
Chemical Physics 333 (2007) 157–167
Chemical Physics
www.elsevier.com/locate/chemphys

Time-dependent density functional calculations of phosphorescence parameters for *fac*-tris(2-phenylpyridine) iridium

Emil Jansson [a,*], Boris Minaev [a], Sigurd Schrader [b], Hans Ågren [a]

[a] *Theoretical Chemistry, Royal Institute of Technology, SE-106 91 Stockholm, Sweden*
[b] *Technische Fachhochschule Wildau, University of Applied Sciences, D-15745 Wildau, Germany*

Received 12 September 2006; accepted 22 January 2007
Available online 4 February 2007

Abstract

fac-Tris(2-phenylpyridine) iridium [*fac*-Ir(ppy)$_3$] produces strong phosphorescence and has therefore been used as materials in organic light emitting diodes to overcome the efficiency limit imposed by the formation of triplet excitons. Accounting for this circumstance we present in this paper a theoretical study of phosphorescence in the Ir(ppy)$_3$ complex. The spin–orbit coupling effects and the radiative lifetime in the high temperature limit (τ) are calculated by time-dependent density functional theory using quadratic response technology in order to elucidate the main mechanism of the phosphorescence. It is found that the orbital structure of the T_1 state has a localized character and that the $T_1 \rightarrow S_0$ transition is determined mostly by charge transfer from one of the ligands to the metal. At the vertical $S_0 \rightarrow T_1$ excitation the triplet state is highly delocalized among all three ligands and has a mixed $\pi\pi^*$ and metal-to-ligand charge transfer character. The intensity borrowing from the S_0 to S_5 transitions is mostly responsible for the strong phosphorescence emission from the *x* and *y* spin sublevels. Our results concord with the experimental data on temperature and magnetic field dependence of the phosphorescence kinetics. The calculated radiative lifetime in the high temperature limit agrees well with the measured decay times (2 μs) accounting for negligible non-radiative quenching of the lowest triplet state.

Keywords: Ir(ppy)$_3$; Phosphorescence; OLED; DFT

1. Introduction

Organic conjugated polymers, like polyparaphenylene vinylene, are used in organic light emitting diodes (OLED) as they lend the possibility to create charge carrier recombination and formation of excitons with high efficiency of light emission [1]. The typical OLED device consists of a layer of a luminescent organic polymer sandwiched between two electrodes. Electrons and holes are first injected from the electrodes into the polymer layer. These charge carriers migrate through the organic layer and form excitons when non-geminate pairs of oppositely charged polarons capture each other. Since the charge pairs are non-geminate they have random spin orientation and the singlet and triplet colliding pairs are equally probable. The triplet state has three spin projections ($M_S = 0, \pm 1$) and the singlet has only one ($M_S = 0$) microstate. Consequently, it has been assumed that the quantum yield has an upper statistical limit of 25%. It has been suggested from both theoretical [2] and experimental work [3] that the ratio between the formation of singlet and triplet excitons, σ_S/σ_T, may exceed 1 and thus the efficiency can go beyond the so-called statistical upper limit. Here it should be noted that recently Lupton et al. [4] have questioned whether this ratio really can exceed the statistical limit. The key issue is that the singlet excitons often provide intense luminescence in conjugated organic species. The luminescence from the triplet excitons, on the other hand, are much less intense since triplet–singlet transitions in organic polymers are six to eight orders of magnitude weaker. They gain dipole

* Corresponding author.
E-mail address: emil@theochem.kth.se (E. Jansson).

0301-0104/$ - see front matter © 2007 Elsevier B.V. All rights reserved.
doi:10.1016/j.chemphys.2007.01.021

activity through spin–orbit coupling (SOC), a perturbation that is very weak by two reasons: (1) the orbital angular momentum between the $\pi\pi^*$ states of conjugated chromophores is almost quenched and (2) the absence of heavy elements in the pure organic system.

In order to compel the triplet excitons to do useful work in OLEDs one needs to add dyes with heavy elements which will participate in the charge carrier recombination and at the same time provide strong SOC in order to overcome the spin-forbiddness of the $T_1 \rightarrow S_0$ transition. Such composite materials constitute an important class of organic polymers, which are doped by a heavy-atom containing dye in order to increase the electroluminescence of the OLEDs [2,5–9]. Such electroluminescence has attracted wide interest because of the strong potential for applications in display devices [9,2]. In particular, the organometallic complex $Ir(ppy)_3$ (*fac*-tris(2-phenylpyridine) iridium) has become very popular because of its strong green phosphorescence [5,6,10]. Incorporation of $Ir(ppy)_3$ into a polymer leads to an attractive OLED material by two reasons: (a) the high rate of electron–hole recombination on the $Ir(ppy)_3$ dye and (b) the relatively strong spin–orbit coupling at the metal center, which induces fast intersystem crossing (ISC) and a highly competitive $T_1 \rightarrow S_0$ radiative transition probability. Moreover, the green color of $Ir(ppy)_3$ phosphorescence (514 nm) is well suited for its use in full color displays. The color can be tunable by applied magnetic fields and temperature changes [10].

The aim of the present paper is to calculate the optical properties of the $Ir(ppy)_3$ complex because of its fundamental significance for OLED applications [6], and because the first principle theoretical analysis of phosphorescence of organometallic compounds now has become a realistic proposition. We present connections between features of electronic structures and photophysical properties including phosphorescence efficiency and energy transfer mechanisms of the $T_1 \rightarrow S_0$ transition of $Ir(ppy)_3$. The electric dipole moments are in the present work calculated by time-dependent density functional theory (TDDFT) using quadratic response (QR) functions in order to interpret the high efficiency of the OLEDs containing these specimen.

2. Methodologies

The phosphorescence lifetime from one of the three sublevels (indexed by k) of the lowest triplet state $|T_1^k\rangle$ is given by

$$\frac{1}{\tau_k} = \frac{4}{3t_0}\alpha_0^3(\Delta E^k)^3 \sum_{\alpha\in\{x,y,z\}} |M_\alpha^k|^2, \tag{1}$$

where $t_0 = (4\pi\epsilon_0)^2\hbar^3/m_e e^4$, α_0 is the fine-structure constant, ΔE^k is the transition energy from the ground state to the $|T_1^k\rangle$ state, and M_α^k is the α-axis projection of the electric dipole transition moment between the ground state and the k-spin level of the triplet state. The radiative lifetime τ of the triplet state in the high-temperature limit, i.e. when spin relaxation equalizes sublevel population before emission, is obtained by averaging over the three sublevels according to

$$\frac{1}{\tau} = \frac{1}{3}\sum_{k=1}^{3}\frac{1}{\tau_k} \tag{2}$$

In order to evaluate Eq. (1) we must calculate the excitation energies and the electric dipole transition moments. The excitation energies can be determined from the poles of the ground state linear polarization propagator

$$\det\left[E^{[2]} - \hbar\omega S^{[2]}\right] = 0, \tag{3}$$

where $E^{[2]}$ and $S^{[2]}$ are the electronic Hessian and overlap matrices, respectively. This approach disregards zero-field splittings of the sublevels of the triplet state. This must be taken into account when evaluating the phosphorescence since it has been shown that the zero-field splitting in $Ir(ppy)_3$ [10] is not negligible. The transition moments can be straightforwardly identified from the residues of Eq. (3), as long as we are interested in singlet–singlet transitions. In case of singlet–triplet transitions the zeroth-order contribution vanishes due to spin-orthogonality. The first contribution to the transition moment then comes from the first-order corrected wave functions. The sublevels of the triplet state are considered to be energy degenerate, so the final expression reduces to

$$M_\alpha^k = \sum_{n=0}^{\infty}\frac{\langle S_0|\hat{\mu}_\alpha|S_n\rangle\langle S_n|\widehat{H}_{SO}|T_1^k\rangle}{E(S_n)-E(T_1)} + \sum_{n=1}^{\infty}\frac{\langle S_0|\widehat{H}_{SO}|T_n\rangle\langle T_n|\hat{\mu}_\alpha|T_1^k\rangle}{E(T_n)-E(S_0)}, \tag{4}$$

where $\widehat{H}_{SO}$ is an electronic spin–orbit operator and the summation over intermediate triplet states includes all three sublevels of each triplet state. The representation of the triplet sublevels can be done in terms of the spin eigenfunctions with M_S as a good quantum number, but, since only the averaged lifetime is of interest (Eq. (2)), any orthonormal set will do and the Cartesian components are often used in this respect. Eq. (4) can be evaluated computing the single residue of the QR, we referee to Ref. [11] for details.

The spin–orbit operator in Eq. (4) we have used is the semi-empirical effective single-electron spin–orbit operator suggested by Koseki et al. [12,13]. This approximation has been thoroughly evaluated in a previous paper [14] where the assessment of all-electron basis sets as well as effective core potentials (ECP) was made. The use of this combination reduces the number of electrons and removes the two-electrons spin–orbit integrals, which greatly facilitates the calculations. It has been shown that the parameterized single-electron SOC operator combined with the use of ECPs can give phosphorescence lifetimes that are within 15% of the values obtained by a full relativistic four-component model [14]. All single-electron spin–orbit coupling integrals including two-center contributions from

metal and all ligands are taken into account in this approach [12,13].

3. Computational details

The molecular structures of $Ir(ppy)_3$, more specifically *fac*-$Ir(ppy)_3$, were optimized at the singlet ground state (S_0) and first excited triplet state (T_1) without symmetry constraints. This was done at the density functional theory (DFT) level using the hybrid B3LYP exchange-correlation functional [16] and Lanl2DZ basis sets [17] adopting the Berny optimization algorithm as implemented in the Gaussian 03 program [18]. For the calculations of excitation energies and transition moments we have used several different basis sets for the light elements (H, C, O); 3-21G [19], 6-31G* [20] and 6-311G* [21], and the Stuttgart ECP basis sets (SDD) [22] for Ir. Structure optimizations were performed with the Gaussian 03 program, [18] property calculations were performed with the Dalton program [23].

4. Results and discussion

4.1. Structure of S_0 and T_1

In the present work we are mostly interested in the structure of the S_0 and the T_1 state since both are involved in the phosphorescence process. Relevant bond lengths are gathered in Table 1 (see Fig. 1 for labeling of atoms) where also bond lengths for S_0 obtained through X-ray diffraction in a number of experimental studies [24–26] are included for comparison. The effective core potential basis set Lanl2DZ provides bond distances for the ground state which are all almost within 0.02 Å of those obtained through X-ray diffraction, e.g. Ir–N (2.151 Å) and Ir–C (2.035 Å) compared to the experimental values from Ref. [26] of 2.132 and 2.024 Å. Our geometry optimization assigns the $Ir(ppy)_3$ complex very closely to C_3 symmetry, with the z-axis actually coinciding with the C_3 axis. Unfortunately, we have not found any reported bond lengths for the T_1 structure. Comparing the changes in bond length of the optimized S_0 and T_1 structures we notice that one of the ligands comes closer to the central Ir-atom and the other two get pushed away. At the same time some internal deformations in this ligand occurs, see Table 1. It seems that the molecule undergoes a rather significant structural change during the S_0–T_1 transition. The changes in bond length can be understood by looking at the molecular orbital (MO) plots, Fig. 2, which tell us that the $S_0 \rightarrow T_1$ transition constitutes a charge transfer from the 5d metal orbital to the ligands. After relaxation at the triplet state the electron distribution localizes at one of the ligands, which then moves closer to the iridium atom. This transition was assigned by Hay [27] as having a metal-to-ligand charge transfer (MLCT) character in which he only considered the vertical $S_0 \rightarrow T_1$ excitation. In fact the "metal" orbital has only 52% of $Ir(5d_{z^2})$ character with the reminder of the orbital being localized at the π-AO's of the ligands; mostly at the phenyl parts of all three ppy ligands, the pyridine parts being practically empty (Fig. 2a). The LUMO orbital at the S_0-ground state geometry has no metal contribution and includes the fully delocalized π-MO's of all ligands (Fig. 2b); it has bonding character in respect to the phenyl-pyridine C–C link.

Since we presently address the $T_1 \rightarrow S_0$ transition we need also to eludicate the molecular orbitals at the T_1-state optimized geometry. In Fig. 3 we have visualized the relevant molecular orbitals for this transition, i.e. the lower and higher lying molecular orbitals of the open shell at the T_1-state optimized geometry. By looking at the molecular orbital plots we can assign $T_1 \rightarrow S_0$ as a ligand-to-metal charge transfer with a strong localization of the higher lying molecular orbital at one of the ligands (ppy1). The spin density at the optimized geometry of the T_1 state is mostly localized at this ligand (and at the metal). Comparison with Nozaki's result (distribution of hole and electron in T_1 state, Table 2 in Ref. [15]) indicates that geometry optimization in Ref. [15] provides some rather different geometry for the T_1 state. The electron and the hole are delocalized through all ligands with partial concentration of the hole on the phenyl part of the ppy1 and on the metal; the electron is more localized on the ppy1 [15]. Thus the T_1 state geometry obtained by Nozaki is somehow intermediate between our T_1 state structure and the ground state geometry.

Table 1
Bond lengths (Å) for the ground (S_0) and the first triplet excited state (T_1)

	T_1	S_0				
	Calc.	Calc.	Calc.[a]	Exp.[b]	Exp.[c]	Exp.[d]
$Ir–N_2$	2.176	2.154	2.167	2.088	2.086	2.132
$Ir–N_{11}$	2.169	2.153	2.167	2.088	2.086	2.132
$Ir–N_{22}$	2.116	2.151	2.167	2.088	2.086	2.132
$Ir–C_{33}$	2.048	2.035	2.035	2.006	2.034	2.024
$Ir–C_{44}$	2.030	2.035	2.035	2.006	2.034	2.024
$Ir–C_{55}$	2.000	2.035	2.035	2.006	2.034	2.024
$N_2–C_7$, $N_{22}–C_{27}$, $N_{11}–C_{16}$	1.36	1.36	–	1.345	1.379	–
$N_2–C_3$, $N_{11}–C_{12}$	1.38	1.38	–	1.358	1.378	–
$N_{22}–C_{23}$	1.439	1.381	–	1.358	1.378	–
$C_{33}–C_{34}$, $C_{44}–C_{45}$, $C_{55}–C_{56}$	1.42	1.42	–	1.405	1.415	–
$C_{33}–C_{38}$, $C_{44}–C_{49}$	1.43	1.44	–	1.423	1.391	–
$C_{55}–C_{60}$	1.485	1.436	–	1.423	1.391	–
$C_3–C_{49}$, $C_{12}–C_{38}$	1.47	1.47	–	–	–	–
$C_{60}–C_{23}$	1.419	1.467	–	–	–	–

First two columns correspond to the calculated values using the B3LYP/Lanl2DZ approach.
[a] Ref. [27].
[b] Ref. [25].
[c] Ref. [24].
[d] Ref. [26].

4.2. Phosphorescence of $Ir(ppy)_3$

In the present work we have by the QR TDDFT technique calculated the S_0–T_1 transition moment as a function of displacement with respect to the ground state equilibrium structure. In Table 2 we present the phosphorescence radiative lifetime (τ) calculated with different basis sets for

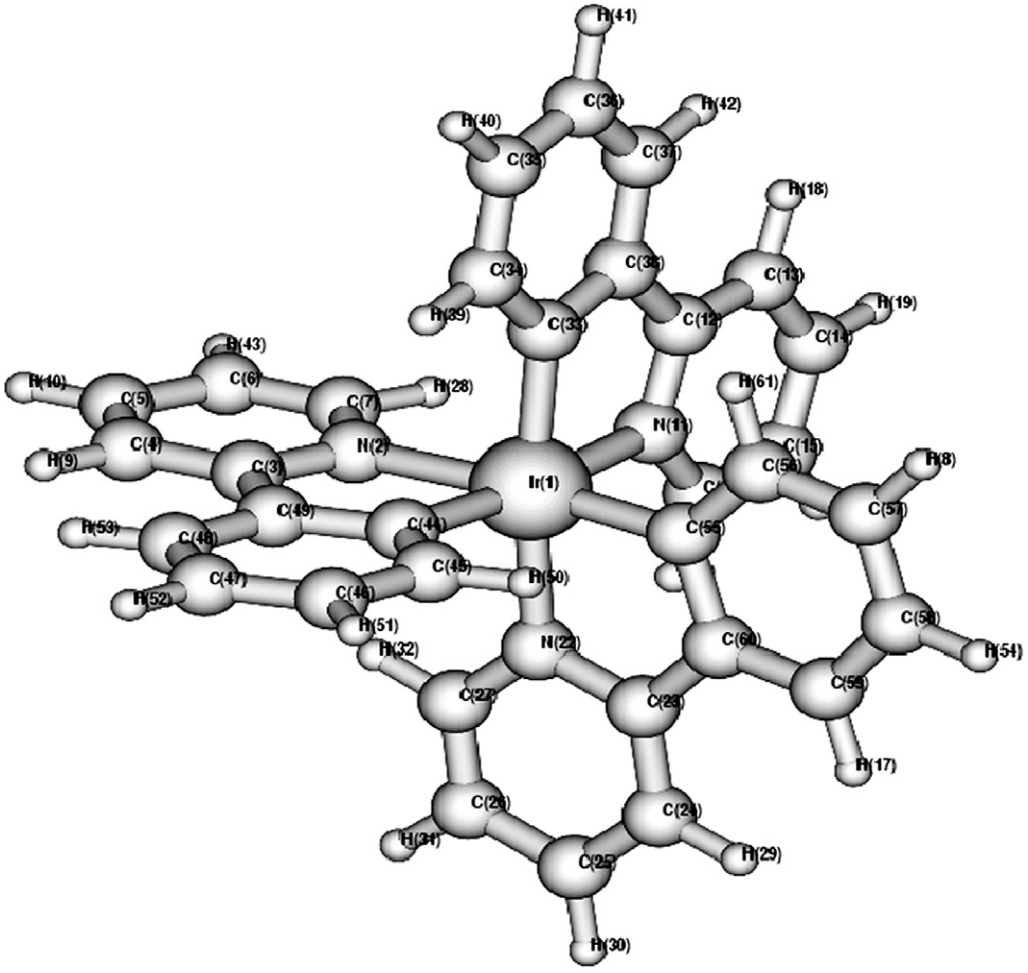

Fig. 1. Structure and labeling for the $Ir(ppy)_3$ molecule.

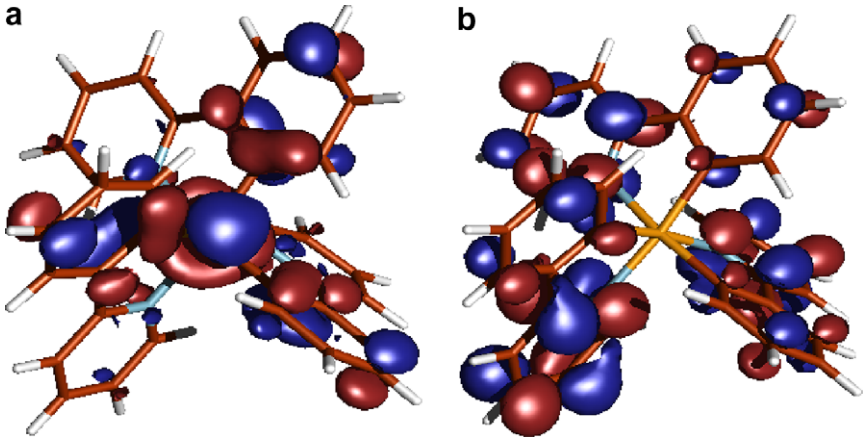

Fig. 2. Molecular orbitals of $Ir(ppy)_3$ at the S_0 optimized geometry: (a) HOMO and (b) LUMO.

the ligands. It seems to be natural to calculate τ at the T_1 state optimized geometry, but since the final state is the ground state which determines the vibronic structure of the emission spectrum it is also useful to consider the S_0–T_1 transition probability at the S_0-optimized geometry. The calculated S_0–T_1^k transition dipole moments for the three spin sublevels ($k = x, y, z$) of the T_1 state at the S_0 optimized geometry and at the first excited triplet state optimized geometry are presented in Table 3. Each spin sublevel provides its own polarization for the S_0–T_1 transition.

Scrutinizing the results we first notice that the small basis set reproduces the same trend for the phosphorescence lifetime for different sublevels as the calculations

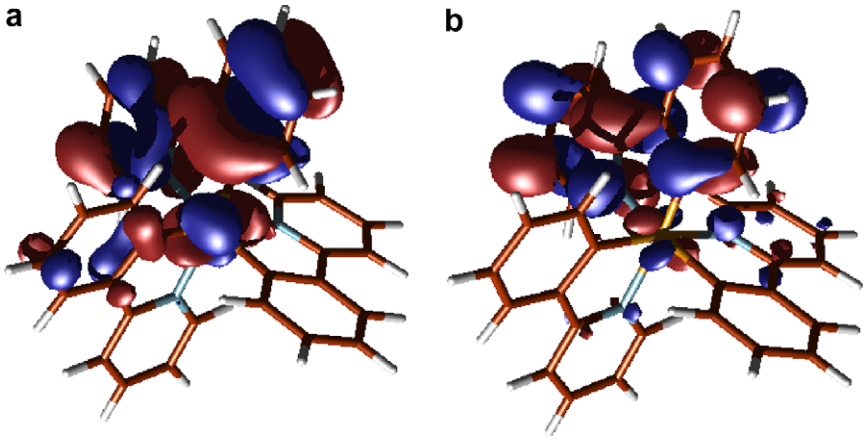

Fig. 3. Molecular orbitals of $Ir(ppy)_3$ at the T_1 optimized geometry: (a) lower lying occupied open shell molecular orbital and (b) upper lying occupied open shell molecular orbital.

performed using the double- and triple-ζ basis sets. The differences in the excitation energy and phosphorescence lifetime are small, indicating basis set convergence of the results. One can expect that diffuse functions (not tested) are not essential owing to the valence nature of the T_1 state. In order to further evaluate the basis set used we have compared our results with previous reported excitation energies for the $S_0 \rightarrow T_1$ and $S_0 \rightarrow S_n$ transitions reported by Hay [27] who used the lanl2DZ basis set combined with the 6-31G. For ten singlet and triplet excited states at the S_0-optimized geometry we reproduce his numbers very well using the SDD ECP and 6-311G* basis set. The $S_0 \rightarrow T_1$ transition is reported by Hay [27] to be 2.59 eV compared to our result of 2.50 eV. Nozaki has calculated the deexcitation energy for the $S_0 \leftarrow T_1$ transition at the T_1-optimized geometry to be close to 2.1 eV (from Table 5 of Ref. [15]), we have calculated this energy to be equal to 2.07 eV. These energies should be compared to the experimentally observed absorption at 2.75 eV and emission at 2.42 eV [28,10].

Comparison with experiment should be qualified taking several factors into consideration. In our calculations we do not include any environmental effects, such as solvent and the presence of other solutes. Furthermore we have not incorporated so far any effect of vibronic coupling on the phosphorescence rate, which indeed is an approximation. The $Ir–C_{55}$ and $Ir–N_{22}$ displacements for the excited ligand (ppy1) is the most important vibrational mode in this respect. These bonds are shortened by 0.035 Å upon the $S_0 \rightarrow T_1$ transition (Table 1). A potential energy surface cross section along this vibrational mode indicates a large force constant in the ground state ($k = 5.54$ mDyne/Å) it is 2.4 times smaller in the T_1 state. A shallow minimum in the triplet state with an essentially anharmonic potential near the equilibrium (as follows from our DFT simulation) and a strongly bound harmonic potential in the ground S_0 state (Fig. 4) lead to the following qualitative conclusions about the S_0–T_1 transitions in absorption and emission.

Table 3
S_0–T_1 transition moment $M_\alpha(T^k)$ calculated with B3LYP/6-311G/SDD[a] at the S_0 and T_1 optimized geometry

Transition moment (sublevel)	S_0	T_1
$M_x(T^x)$	−0.008	0.078
$M_y(T^x)$	−0.211	−0.105
$M_z(T^x)$	−0.013	−0.002
$M_x(T^y)$	0.210	0.063
$M_y(T^y)$	−0.014	−0.055
$M_z(T^y)$	0.006	0.001
$M_x(T^z)$	0.015	0.053
$M_y(T^z)$	−0.011	−0.059
$M_z(T^z)$	0.018	−0.002

α corresponds to the direction of the dipole transition moment and k corresponds to the cartesian component of the ZFS triplet state spin sublevel.

[a] 6-311G* used on light elements (H, C, O) and SDD on Ir.

Table 2
Radiative phosphorescence lifetimes for the three spin sublevels τ_α (μs) of the $Ir(ppy)_3$ complex calculated with B3LYP QR method using various basis sets on light atoms (H, C, O), SDD has been used on Ir during all calculations

Basis set	S_0					T_1				
	$\Delta E_{S–T}$	τ_x	τ_y	τ_z	τ	$\Delta E_{S–T}$	τ_x	τ_y	τ_z	τ
3-21G	2.513	0.772	0.768	43	1.15	2.102	3.701	8.160	11.092	6.21
6-31G*	2.516	1.32	1.32	82.74	1.96	2.082	6.057	14.776	16.365	10.21
6-311G*	2.503	1.34	1.34	88.01	2.00	2.068	6.220	15.071	16.948	10.48

τ (μs) is the radiative phosphorescence lifetime in the high-temperature limit. $\Delta E_{S–T}$ (eV) is the S_0–T_1 excitation energy. Calculations have been performed at the S_0 and T_1 optimized geometry.

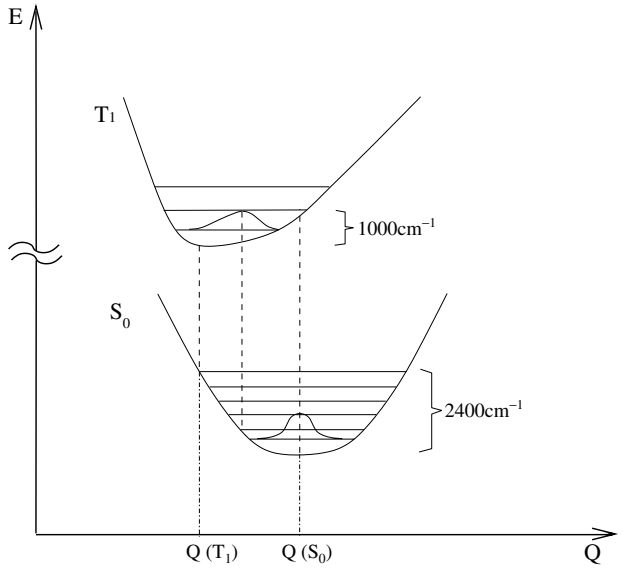

Fig. 4. Potential energy surfaces for $Ir(ppy)_3$.

The phosphorescence from the lowest vibrational level at low temperature (1.4 K) should be very broad (half width of about 3000 cm^{-1} is detected and site selective excitation did not lead to any significant spectral narrowing in solid THF solvent [10]).

Since there is a large displacement in the equilibrium positions the maximum of the $S_0 \rightarrow T_1$ transition in absorption should be shifted to higher energy ($v'' = 0 \rightarrow v' = 4$ transition). Accounting for the shallow minimum and the anharmonicity of the upper state potential we can predict that the zero vibrational level of the T_1 curve will have a maximum of its vibrational wave function somewhere in the middle of the S_0 and T_1 equilibrium positions. Thus, all calculated properties of phosphorescence would be somehow intermediate between results calculated at the S_0 and T_1 optimized geometries.

In order to understand the mechanism of the phosphorescence we have adopted the following scheme: first we calculated the excitation energies and transition moments using the single residue of the quadratic response function. Secondly, we calculated the matrix elements and energies for the sum-over-states expression (Eq. (4)) for $n = 10$. By comparing these two sets of calculations we can evaluate how much of the total transition moment is obtained from the first ten singlet and triplet states. If the main part of the total transition moment is collected from these states we can make a quantitative analyze of how much each of them contributes to the total transition intensity. We use the zero-field spin functions,

$$t^x = \frac{1}{\sqrt{2}}[\beta\beta - \alpha\alpha], \quad t^y = \frac{\mathrm{i}}{\sqrt{2}}[\beta\beta + \alpha\alpha],$$
$$t^z = \frac{1}{\sqrt{2}}[\alpha\beta + \beta\alpha] \tag{5}$$

which are fixed with respect to the chosen molecular axes.

In Tables 4–7 we have collected electric dipole transition moments, SOC matrix elements and excitation energies for the ten low-lying singlet and triplet states which contribute to the phosphorescence intensity in Table 2. Performing the sum-over-state analysis we manage to sum up the major part of the intensity for all interesting pathways of the intensity borrowing except the transition moment along the x-axis to the x-sublevel ($M_x(x)$), see Tables 8 and 9. Since the spin sublevels of the T_1 state mostly provides x- and y-polarized phosphorescence we have excluded the z-polarized contributions from Tables 8 and 9. Looking at Tables 4–7 we can draw the following conclusion based on the scheme mentioned above; for phosphorescence the S_2, S_3, S_4 and especially S_5 states are important as they provide large SOC with the T_1 state allowing the S_0–T_1 transition to steal intensity from the singlet–singlet transitions. Other important states are T_2, T_4 and T_5, which have large SOC mixing with the ground state; this leads to intensity

Table 4
Electric dipole transition moment (a.u.) for S_0–S_n transitions and excitation energy $\Delta E_k = E(S_k) - E(S_0)$ (eV) calculated with B3LYP/6-311G*/SDD[a] at the S_0 optimized geometry

State k	Trans. moment			ΔE_k		f	
	$\langle S_0\|\hat{\mu}_x\|S_k\rangle$	$\langle S_0\|\hat{\mu}_y\|S_k\rangle$	$\langle S_0\|\hat{\mu}_z\|S_k\rangle$	Calc.	Calc.[c]	Calc.	Calc.[c]
0[b]	0.068	0.161	−2.445	–			
1	0.021	0.023	−0.286	2.745	2.80	0.0056	0.0044
2	−0.157	−0.085	−0.018	2.804	2.85	0.0022	0.0019
3	0.095	−0.158	−0.012	2.805	2.85	0.0023	0.0022
4	0.473	0.347	0.026	2.980	3.03	0.0252	0.0207
5	0.354	−0.481	−0.008	2.983	3.04	0.0260	0.0186
6	−0.016	−0.047	−0.195	2.998	3.04	0.0030	0.0058
7	−0.289	0.779	0.045	3.091	3.14	0.0525	0.0601
8	−0.788	−0.290	−0.039	3.092	3.15	0.0536	0.0617
9	0.038	−0.031	0.094	3.102	3.18	0.0008	0.0504
10	0.021	0.056	−0.768	3.309	3.39	0.0481	0.0067

[a] 6-311G* used on light elements (H, C, O) and SDD on Ir.
[b] Permanent electric dipole moment.
[c] Ref. [27].

Table 5
Electric dipole transition moment (a.u.) for the T_1–T_n transitions and excitation energy $\Delta E_k = E(T_k) - E(S_0)$ (eV) calculated with B3LYP/6-311G*/SDD[a] at the S_0 optimized geometry

State k	Trans. moment			ΔE_k	
	$\langle T_1\|\hat{\mu}_x\|T_k\rangle$	$\langle T_1\|\hat{\mu}_y\|T_k\rangle$	$\langle T_1\|\hat{\mu}_z\|T_k\rangle$	Calc.	Calc.[c]
1[b]	−0.102	0.194	−0.688	2.503	2.59
2	−0.535	0.876	0.039	2.519	2.60
3	0.788	0.446	0.054	2.522	2.60
4	−0.076	−0.021	0.035	2.737	2.79
5	−0.545	0.230	−0.001	2.775	2.83
6	−0.220	−0.488	−0.042	2.775	2.83
7	0.016	−0.572	−0.025	2.892	2.95
8	0.565	−0.029	0.029	2.892	2.95
9	−0.006	−0.032	0.146	2.930	2.98
10	−0.007	−0.060	0.397	3.001	3.10

[a] 6-311G* used on light elements (H, C, O) and SDD on Ir.
[b] Permanent electric dipole moment.
[c] Ref. [27].

Table 6
SOC matrix elements (10^{-3} a.u.) calculated with B3LYP/6-311G*/SDD[a] at the S_0 optimized geometry

State k	Matrix element		
	$\langle S_k\|\hat{H}^x_{SO}\|T_1\rangle$	$\langle S_k\|\hat{H}^y_{SO}\|T_1\rangle$	$\langle S_k\|\hat{H}^z_{SO}\|T_1\rangle$
0	−0.170	−0.039	−0.632
1	0.111	−0.040	−0.025
2	−0.556	0.474	0.013
3	−0.454	−0.430	−0.016
4	−2.769	3.151	0.198
5	3.067	2.545	0.310
6	0.114	0.071	0.254
7	−1.155	−0.810	−0.212
8	0.373	−1.002	−0.096
9	−0.041	−0.027	−0.514
10	−0.075	−0.070	−0.671

[a] 6-311G* used on light elements (H, C, O) and SDD on Ir.

Table 7
SOC matrix elements (10^{-3} a.u.) calculated with B3LYP/6-311G*/SDD[a] at the S_0 optimized geometry

State k	Matrix element		
	$\langle S_0\|\hat{H}^x_{SO}\|T_k\rangle$	$\langle S_0\|\hat{H}^y_{SO}\|T_k\rangle$	$\langle S_0\|\hat{H}^z_{SO}\|T_k\rangle$
1	−0.170	−0.039	−0.632
2	−2.003	−0.607	−0.044
3	−0.623	1.999	0.107
4	−0.050	−0.165	1.467
5	−1.321	−0.532	−0.137
6	0.555	−1.315	−0.115
7	1.525	0.793	0.061
8	−0.786	1.541	0.027
9	0.056	0.044	−1.784
10	−0.020	−0.065	0.982

[a] 6-311G* used on light elements (H, C, O) and SDD on Ir.

borrowing from the T_1–$T_{2,4,5}$ transitions. Also, this lets us quantify the importance of each of the 10 first contributing singlet and triplet states. For all transition pathways the intensity borrowing from the S_0–S_k transitions is approximately ten times higher than compared to the intensity stolen from the T_1–T_k transitions. This makes the contributions from the triplet manifold (singlet to triplet spin–orbit and triplet to triplet dipole interactions, second term in Eq. (4)) negligible compared to the contributions from the singlet-manifold (singlet to triplet spin–orbit and singlet to singlet dipole interactions, first term in Eq. (4)). In the singlet manifold the S_2, S_3, S_4 and S_5 states all experience strong SOC to T_1. S_5–S_0 is the strongest transition among them and provides mainly the *x*- and *y*-polarized light for the phosphorescence emission. Thus we predict that the z-polarized phosphorescence cannot be observed.

The electronic S_0–T_1 transition dipole moment is a strong function of the displacement (Fig. 4, Table 3). At the ground state geometry with a symmetry close to the C_3 point group the lowest triplet state (2.503 eV) belongs to the ^{3}A symmetry (orbital part is totally symmetrical) and the next two triplet states are very close in energy (2.52 eV) and are almost degenerate; thus their symmetry is ^{3}E in a good agreement with the result of Hay [27]. Similar results are obtained for the singlet excited states (Table 4).

The phosphorescence lifetimes for spin sublevels presented in Table 2 indicate rather big qualitative and quantitative differences for the two geometrical structures. At the S_0-optimized geometry with C_3 symmetry, emission from the T^x and T^y sublevels of the lowest ^{3}A state provides *y* and *x* polarization (Table 3) with the equally short radiative lifetime (Table 2). The T^z sublevel is almost dark; its radiative lifetime is 66 times longer. Thus at the thermal equilibrium (high temperature limit at T 77 K) the lowest triplet state will be depleted through emission from the T^x and T^y sublevels. The calculated SOC matrix elements $\langle S_0|\hat{H}_{SO}|T_1\rangle$ for T^x and T^y sublevels are 27 and 8.6 cm^{-1}, thus considering the large energy gap ($\Delta E_{T_1,S_0}$), the intramolecular non-radiative quenching of these sublevels should be slow and could not compete with the phosphorescent emission. For the T^z sublevel the SOC matrix

Table 8
Contribution to the S_0–T_1 transition moment from S_0–S_n transitions calculated with B3LYP/6-311G*/SDD[a] at the S_0 optimized geometry

	$n=0$	$n=1$	$n=2$	$n=3$	$n=4$	$n=5$	$n=6$	$n=7$	$n=8$	$n=9$	$n=10$	$\sum_{n=0}^{10}$	M_α
$M_x(T^x)$	0.000	0.000	0.008	−0.004	−0.075	0.062	0.000	0.016	−0.014	0.000	−0.000	−0.007	−0.008
$M_y(T^x)$	0.000	0.000	0.004	0.007	−0.055	−0.084	0.000	−0.042	−0.005	0.000	−0.000	−0.175	−0.211
$M_x(T^y)$	0.000	0.000	−0.007	−0.004	0.085	0.051	0.000	0.011	0.037	0.000	−0.000	0.173	0.210
$M_y(T^y)$	0.000	0.000	−0.004	0.006	0.063	−0.070	0.000	−0.029	0.013	0.000	−0.000	−0.021	−0.014
$M_x(T^z)$	0.001	0.000	−0.000	−0.000	0.005	0.006	0.000	0.003	0.004	−0.001	−0.001	0.016	0.015
$M_y(T^z)$	0.001	0.000	−0.000	0.000	0.004	−0.009	−0.001	−0.008	0.001	0.000	−0.001	−0.011	−0.011

α corresponds to the direction of the dipole transition moment and k to the cartesian component of the ZFS triplet state spin sublevel. M_α is the total transition moment to the corresponding spin sublevel.
[a] 6-311G* used on light elements (H, C, O) and SDD on Ir.

Table 9
Contribution to the S_0–T_1 transition moment from T_1–T_n transitions calculated with B3LYP/6-311G*/SDD[a] at the S_0 optimized geometry

	$n=1$	$n=2$	$n=3$	$n=4$	$n=5$	$n=6$	$n=7$	$n=8$	$n=9$	$n=10$	$\sum_{n=0}^{10}$	M_α
$M_x(T^x)$	0.000	0.012	−0.005	0.000	0.007	−0.001	0.000	−0.004	0.000	0.000	0.008	−0.008
$M_y(T^x)$	−0.000	−0.019	−0.003	0.000	−0.003	−0.003	−0.008	0.000	0.000	0.000	−0.036	−0.211
$M_x(T^y)$	0.000	0.004	0.017	0.000	0.003	0.003	0.000	0.008	0.000	0.000	0.035	0.210
$M_y(T^y)$	−0.000	−0.006	0.010	0.000	−0.001	0.006	−0.004	−0.000	0.000	0.000	0.004	−0.014
$M_x(T^z)$	0.001	0.000	0.001	−0.001	0.001	0.000	0.000	0.000	0.000	0.000	0.002	0.015
$M_y(T^z)$	−0.001	−0.000	0.001	−0.000	−0.000	0.001	−0.000	−0.000	0.001	−0.001	−0.002	−0.011

α corresponds to the direction of the dipole transition moment and k to the cartesian component of the ZFS triplet state spin sublevel. M_α is the total transition moment to the corresponding spin sublevel.
[a] 6-311G* used on light elements (H, C, O) and SDD on Ir.

element with the ground state is higher (138.7 cm^{-1}), but its non-radiative relaxation still is slower than the radiative decay from the thermolized triplet state as follows from our estimations according to simple theory [10]. In this case the calculated averaged τ value (Eq. (2)) should be close to the observed phosphorescence lifetime in the high temperature limit. In fact the τ value calculated with large basis set at S_0 geometry (2 μs, Table 2) is in a good agreement with the measured phosphorescence decay time for $Ir(ppy)_3$ in degassed acetonitrile at 300 K (1.9 μs) [10,29], in degassed toluene and in tetrahydrofuran at 130 K (2 μs) [10].

The S_0–$T_1^{x,y}$ transition moments calculated at the T_1 state optimized geometry are essentially smaller (Table 3) and the radiative lifetimes are, respectively, longer than at the ground state structure. For the largest basis set we obtain $\tau = 10.5$ μs which is approximately five times longer than the experimental reported lifetimes (about 2 μs [10,29,30]). At the T_1 state optimized geometry the complex has no C_3 symmetry any more because of the strong distortion for one ligand (ppy1); in this case the T^x sublevel is more active in phosphorescence than the T^y and T^z substates (Table 2), but the spin selectivity is not so high as before. All calculations predict that z-polarization of the phosphorescent emission is almost negligible (Table 3).

Accounting for the shallow minimum and the anharmonicity of the lowest triplet T_1 state potential (Fig. 4) we can see that the $v = 0$ vibrational level wave function of the phosphorescent state provides a maximum density of probability at some intermediate geometry (between the S_0 and T_1 states structures). The dependence of the S_0–T_1^k transition moments on the displacement mode, $M^k(Q)$, is quite strong (Table 3) and indicates an increase at the S_0 geometry. One can anticipate that the vibrational averaged 0–0 transition moment would be close to the M^k value at the ground state structure.

In order to compare the calculated phosphorescence parameters with experimental data [10] in more detail we need to consider the zero-field splitting (ZFS) in the triplet T_1 state [31–34] and the ZFS influence on the detected lifetime. Spin–spin coupling provides a negligible contribution to ZFS in the $Ir(ppy)_3$ complex in comparison with the SOC contributions, which have been calculated in terms of variational treatment and also by the second-order perturbation theory (the 10 lowest singlet and triplet have been taken into account). For the S_0 geometry perturbation theory is not applicable, because the T_1–T_2 energy gap is comparable with the SOC matrix element, therefore we use a variational treatment. The results are presented in Table 10 for the S_0 and T_1 states geometries. The ZFS calculation indicates that the "dark" spin sublevel T^z is the lowest one

Table 10
ZFS sublevels (cm^{-1}) for the T_1 state for $Ir(ppy)_3$ calculated with B3LYP/6-311G*/SDD[a] at the S_0 and T_1 optimized geometry

T_1 sublevel	S_0-geometry	T_1-geometry
z	19989.06	16609.87
y	20021.79	16663.47
x	20092.98	16678.48

[a] 6-311G* used on light elements (H, C, O) and SDD on Ir.

in both cases. This agrees with the results of temperature effect studies on the phosphorescence decay dynamics [10]. (In Nozaki paper [15] the free-fold axis of the ground state structure is denoted as the *y*-axis; it also corresponds to the lowest ZFS sublevel in agreement with observations [10]).

In the case of the weak $T_1^z \rightarrow S_0$ transition at the geometry of the $Ir(ppy)_3$ complex close to the ground state structure, vibronic coupling is of particular importance, since it can provide additional enhancement of the transition probability [35,36]. The most important in this case is the so-called Herzberg–Teller (HT) mechanism, which is determined by the $\partial M^k(Q)/\partial Q$ derivatives. Non-totally symmetric vibrational modes are usually active in the HT mechanism of the $T_1 \rightarrow S_0$ transition enhancement. The ground state vibrations and corresponding symmetry selection rules have to be used (the C_3 symmetry point group). The above-mentioned displacement (Fig. 4) corresponds to one of most active vibrational modes in the HT mechanism. But there are a few other modes which include metal–ligand and intraligand vibrations, which are proposed to be active in the HT enhancement of the weak $T_1^z \rightarrow S_0$ transition. Thus emission to the vibrational satellites of the ground S_0 state (false origin) at very low temperature (1.5 K) will include mostly vibronic transitions from the lowest T^z spin sublevel. At this low temperature the spin-lattice relaxation between spin sublevels are governed by the so-called direct process [37] which can compete with phosphorescence; thus thermolization of the triplet manifold is possible. The lowest T^z spin sublevel emits a broad phosphorescence band consisting of a few overlapping vibronic transitions shifted to the red from the 0–0 origin. The spectrum is broad due to overlapping vibronic bands for the HT-active vibrational modes of the complex. Intermolecular vibrations in the solvent cage can also contribute to this emission. Moreover, these broad bands should be smeared out by inhomogeneous broadening [10,32,38].

These results are in agreement with experimental studies of $Ir(ppy)_3$ phosphorescence at different temperatures [10,39,24]. For *fac*-$Ir(ppy)_3$ dissolved in THF the observed maximum of the broad phosphorescence band lies at about 535 nm at low temperature (1.5 K) [10]. With temperature increase to 30–100 K the upper lying $T_1^{x,y}$ spin sublevels are thermally populated and pure electronic 0–0 phosphorescence emission occurs. This leads to the band emerging at shorter wavelength (about 505 nm) [10]. The shift of wavelength is determined by vibrational false origin not by ZFS. The HT mechanism is not important for emission from the $T_1^{x,y}$ spin sublevels, since they have quite large intrinsic (pure electronic) transition probability.

Thus our calculations at the S_0 state geometry do not contradict with results of Finkenzeller and Yersin [10] on the temperature- and magnetic field-induced changes in the phosphorescence spectra and decay rates. A qualitative consideration of Fig. 4 and transition moments calculated at the T_1 state geometry provide some deviation from the simple picture mentioned above. In the former case (the C_3 symmetry point group) the active $T_1^{x,y}$ spin sublevels are close in energy, but the fit to the observed kinetics requires a rather big splitting between the two upper spin sublevels (83 cm^{-1}) [10].

The ZFS of the spin sublevels of the lowest triplet state and their spontaneous emission to the S_0 ground state has to be determined at some intermediate geometry between the optimized S_0 and T_1 states structures, because the upper state potential has strongly anharmonic character near the shallow minimum with respect to the M–L displacement. According to the quadratic response calculations the intensity borrowing from the S_0–S_5 transitions carries most of the responsibility for the strong phosphorescence emission from the *x* and *y* spin sublevels. At the same time, the ZFS and mixing of the triplet state sublevel wave functions strongly depend on the energy gaps between the T_1, T_2, and T_3 states which are very close at the ground state geometry (Table 5).

Finkenzeller and Yersin [10] have reported emission spectra and decay times for all three spin sublevels of the first triplet state and obtained $\tau_I = 145$ μs, $\tau_{II} = 11$ μs and $\tau_{III} = 0.750$ μs. They distinguished emission from the three substates by analysis of the temperature- and magnetic field-induced changes in the phosphorescence spectra and decay rates. Finkenzeller and Yersin [10] assumed that the T_1 state has a large zero-field splitting induced by the second-order SOC perturbation as found for many organometallic complexes. They also proposed that spin–vibronic coupling provides specific activity of some non-totally symmetric vibrational mode for emission from the lowest spin sublevel. By these reasonable assumptions they explained the observed spectral shift and intensity changes in the phosphorescent emission spectra induced by temperature and magnetic field variations.

The calculated lifetimes are in reasonable agreement with the kinetic analysis of Ref. [10], except for one of the sublevels that does not match the trend. This can be caused by e.g. displacement in the ppy-ligands which is not taken into consideration since we do not include explicitly the vibronic effects in our calculations. The proper account of anharmonicity of the upper state potential and vibrational averaging of the transition moment probably will improve the agreement with experiment.

4.3. Non-radiative processes

The intersystem crossing (ISC) $S_k \rightsquigarrow T_1$ in $Ir(ppy)_3$ complex is very fast [40]. The SOC matrix elements $\langle S_k|\hat{H}_{SO}|T_1\rangle$ are very large for $k = 2$–5. (Table 6). All these states include high contribution of the M–L CT character and different types of 5d-orbitals, thus they include a strong change of the orbital angular momentum. All these states are also close in energy and can participate in the ISC process and in vibronic mixing. Comparison with the SOC integrals at the triplet state geometry indicates their strong dependence on the M–L distortion and the intraligand displacements. Such spin–vibronic interaction can induce

electronic energy transfer to the vibrational movement, which is necessary for an efficient $S_k \rightarrow T_1$ ISC process [40–42]. All these features support the experimental finding about a very fast ISC in the $Ir(ppy)_3$ complex [40].

On the other hand, the non-radiative quenching of the triplet state $T_1 \rightsquigarrow S_0$ should be rather slow by two reasons: the $\Delta E_{T_1,S_0}$ energy gap is quite big in the $Ir(ppy)_3$ complex (Table 4), and the SOC matrix elements $\langle S_0|\widehat{H}_{SO}|T_1\rangle$ are relatively small (Table 6). This is because the $S_0 \rightarrow T_1$ excitation is connected mostly with the HOMO–LUMO transition; the SOC integral for these orbitals does not include the metal contribution (there is no metal contribution at the LUMO, Fig. 2b). Thus only two-center SOC integrals produce non-zero values. Besides for the HOMO–LUMO excitations there are some small contributions from other excited configurations which also contribute to the $\langle S_0|\widehat{H}_{SO}|T_1\rangle$ matrix element.

5. Conclusion

We have presented time-dependent density functional theory quadratic response calculations of the phosphorescence lifetimes of *fac*-tris(2-phenylpyridine) Iridium [$Ir(ppy)_3$]. The study is motivated by the fact that $Ir(ppy)_3$ has been used as guest dye in organic light emitting diodes (OLED) in order to convert triplet excitons into light emission. We wanted to elucidate the mechanism of the strong electroluminescence by looking for the origin of the triplet state emission. It is found that the orbital structure of the T_1 state has a localized character and that the $T_1 \rightarrow S_0$ transition is determined mostly by charge transfer from one of the ligands to the metal. At the vertical $S_0 \rightarrow T_1$ excitation the triplet state is highly delocalized among all three ligands and has a mixed $\pi\pi^*$ and MLCT character. The zero field spitting of spin sublevels of the lowest triplet state and their spontaneous emission to the S_0 ground state has to be determined at some intermediate geometry between optimized S_0 and T_1 states structures, because the upper state potential has strongly anharmonic character near the shallow minimum with respect to the M–L displacement. According to the quadratic response calculations the intensity borrowing from the S_0–S_5 transitions is mostly responsible for the strong phosphorescence emission from the *x* and *y* spin sublevels. Large spin–orbit coupling is obtained between the T_1 and S_2, S_3, S_4 and S_5 states since all of them have a strong metal to ligand charge transfer character. We conclude that the strong spin–orbit coupling between T_1 and S_5 together with the large dipole interaction between S_5 and S_0 is the reason for the intense phosphorescence of $Ir(ppy)_3$. These strong couplings are absent in the *z*-polarized transition.

Our spin sublevel lifetimes do not completely match the trend obtained by Finkenzeller and Yersin [10], differing in one spin sublevel, something we attribute to neglect of vibronic coupling which is the crude approximation in the current treatment. The overall phosphorescence lifetime in the high temperature limit is still found to be in a good agreement with experiment, indicating that the essentials of the phosphorescence in the investigated system are captured. It is our hope that further theoretical calculations of the kind presented here can help to understand the phosphorescence of known systems and at the same time constitute a tool for building structure–property relationships that can be useful to synthesize even more efficient OLED dyes based on phosphorescence.

References

[1] M.A. Baldo, D.F. O'Brien, Y. You, A. Shoustikov, S. Sibley, M.E. Thompson, S.R. Forrest, Nature 395 (1998) 151.
[2] Z. Shuai, D. Bekjonne, R. Silbey, J. Bredas, Phys. Rev. Lett. 84 (2000) 131.
[3] Y. Cao, I.D. Parker, G. Yu, C. Zhang, A.J. Heeger, Nature 397 (1999) 414.
[4] M. Reufer, M.J. Walter, P.G. Lagoudakis, A.B. Hummel, J.S. Kolb, H.G. Roskos, U. Scherf, J.M. Lupton, Nat. Mater. 4 (2005) 340.
[5] M.A. Baldo, D.F. O'Brien, M.E. Thompson, S.R. Forrest, Phys. Rev. B 60 (1999) 14422.
[6] M.A. Baldo, S.R. Forrest, Phys. Rev. B 62 (2000) 10958.
[7] J. Wilson, A. Dhoot, A. Seeley, M. Khaan, A. Kohler, R. Friend, Nature 413 (2001) 828.
[8] M. Wohlgenannt, K. Tandon, S. Mazumdar, S. Ramasesha, Z. Vardeny, Nature 409 (2001) 494.
[9] Y. Noh, C. Lee, J. Kim, K. Yase, J. Chem. Phys. 114 (2003) 2853.
[10] W.J. Finkenzeller, H. Yersin, Chem. Phys. Lett. 377 (2003) 299.
[11] J. Olsen, P. Jørgensen, J. Chem. Phys. 82 (1985) 3235.
[12] S. Koseki, M.S. Gordon, M.W. Schmidt, N. Matsunaga, J. Chem. Phys. 99 (1995) 12764.
[13] S. Koseki, M.W. Schmidtand, M.S. Gordon, J. Chem. Phys. 102 (1998) 10430.
[14] E. Jansson, P. Norman, B.F. Minaev, H. Ågren, J. Chem. Phys. 124 (2006) 114106.
[15] K. Nozaki, J. Chin. Chem. Soc. 53 (2006) 101.
[16] A. Becke, J. Chem. Phys. 98 (1993) 5648.
[17] P. Hay, W. Wadt, J. Chem. Phys. 82 (1985) 299.
[18] M.J. Frisch, G.W. Trucks, H.B. Schlegel, G.E. Scuseria, M.A. Robb, J.R. Cheeseman, J.A. Montgomery Jr., T. Vreven, K.N. Kudin, J.C. Burant, J.M. Millam, S.S. Iyengar, J. Tomasi, V. Barone, B. Mennucci, M. Cossi, G. Scalmani, N. Rega, G.A. Petersson, H. Nakatsuji, M. Hada, M. Ehara, K. Toyota, R. Fukuda, J. Hasegawa, M. Ishida, T. Nakajima, Y. Honda, O. Kitao, H. Nakai, M. Klene, X. Li, J.E. Knox, H.P. Hratchian, J.B. Cross, C. Adamo, J. Jaramillo, R. Gomperts, R.E. Stratmann, O. Yazyev, A.J. Austin, R. Cammi, C. Pomelli, J.W. Ochterski, P.Y. Ayala, K. Morokuma, G.A. Voth, P. Salvador, J.J. Dannenberg, V.G. Zakrzewski, S. Dapprich, A.D. Daniels, M.C. Strain, O. Farkas, D.K. Malick, A.D. Rabuck, K. Raghavachari, J.B. Foresman, J.V. Ortiz, Q. Cui, A.G. Baboul, S. Clifford, J. Cioslowski, B.B. Stefanov, G. Liu, A. Liashenko, P. Piskorz, I. Komaromi, R.L. Martin, D.J. Fox, T. Keith, M.A. Al-Laham, C.Y. Peng, A. Nanayakkara, M. Challacombe, P.M.W. Gill, B. Johnson, W. Chen, M.W. Wong, C. Gonzalez, J.A. Pople, Gaussian 03, Revision B05, Gaussian, Inc., Pittsburgh, PA, 2003.
[19] J.S. Binkley, J.A. Pople, W.J. Hehre, J. Am. Chem. Soc. 102 (1980) 939.
[20] W.J. Hehre, R. Ditchfield, J.A. Pople, J. Chem. Phys. 56 (1972) 2257.
[21] R. Krishnan, J.S. Binkley, R. Seeger, J.A. Pople, J. Chem. Phys. 72 (1980) 650.
[22] T.H. Dunning Jr., P.J. Hay, in: H. Schaefer (Ed.), Modern Theoretical Chemistry, vol. 2, Plenum, New York, 1976.
[23] Dalton, a molecular electronic structure program, Release 2.0. 2005, see http://www.kjemi.uio.no/software/dalton/dalton.html.
[24] J. Breu, P. Stössel, S. Scrader, A. Starukhin, W.J. Finkenzeller, H. Yersin, Chem. Mater. 17 (2005) 1745.

[25] F.K. Allen, O. Kennard, Chem. Des. Autom. News 8 (1993) 31.
[26] F.O. Garcs, K. Dedeian, N.L. Keder, R.J. Watts, J. Acta Crystallogr. C 49 (1993) 1117.
[27] P.J. Hay, J. Phys. Chem. A 106 (2002) 1634.
[28] K.A. King, P.J. Spellane, R.J. Watts, J. Am. Chem. Soc. 107 (1985) 1431.
[29] K. Dedeian, P.I. Djurovich, F.O. Garces, G. Carlson, R. Watts, Inorg. Chem. 30 (1991) 1685.
[30] K.C. Tang, K.L. Liu, I.C. Chen, Chem. Phys. Lett. 386 (2004) 437.
[31] O. Vahtras, B.F. Minaev, O. Loboda, H. Ågren, K. Ruud, Chem. Phys. 279 (2002) 133.
[32] B.F. Minaev, O. Loboda, O. Vahtras, K. Ruud, H. Ågren, Theor. Chim. Acta 111 (2004) 168.
[33] O. Loboda, I. Tunnell, B.F. Minaev, H. Ågren, Chem. Phys. 312 (2005) 299.
[34] B.F. Minaev, Fizika Molecul, Naukova Dumka, Kiev. 7 (1979) 34.
[35] B.F. Minaev, H. Ågren, Chem. Phys. 315 (2005) 215.
[36] B.F. Minaev, Y-H. Wang, C-K. Wang, Y. Luo, H. Ågren, Spectrochim. Acta A 65 (2006) 308.
[37] H. Yersin, J. Strasser, Coord. Chem. Rev. 208 (2000) 331.
[38] O. Loboda, B. F Minaev, O. Vahtras, H. Ågren, K. Ruud, J. Phys. Chem. 119 (2003) 3120.
[39] T. Tusboi, N. Aljaroudi, Opt. Mater. 27 (2005) 1859.
[40] K.-C. Tang, K. Lin Liu, I-C. Chen, Chem. Phys. Lett. 386 (2004) 437.
[41] G.V. Majer, V.Y. Artuyhov, O.K. Bazyl, in: Electronno-vozbuzhdennyje Sostojanija – Electronic Excited States and Photochemistry of Organic Compounds, Nauka, Novosibirsk, 1997.
[42] P. Macak, Y. Luo, H. Ågren, Chem. Phys. Lett. 330 (2000) 447.